Data supplement for Toll et al., An Electroencephalography Connectomic Profile of Posttraumatic Stress Disorder. Am J Psychiatry (doi: 10.1176/appi.ajp.2019.18080911)

METHODS

Cognitive assessments

A comprehensive, computer-administered neurocognitive battery assessed multiple domains, emphasizing executive functions including working memory, inhibition, and shifting.(1, 2) Working memory was assessed by a digit span forward task in which participants are presented digit sequences of varying length and then asked to enter the sequence in the order presented. The task begins with a sequence of 3 digits (2 iterations at each level) and increments in sequence length until 2 trials at the same level are incorrect or the maximum span of 9 digits is reached. The number of correctly performed sequences was used for analyses. Inhibition was assessed using a go/no go task in which the word "PRESS" was intermittently presented (display time 500ms, ISI 500ms) in either green (126 trials) or red (42 trials) color, requiring the space bar to be pressed as quickly as possible, or the response withheld, respectively. The mean reaction time for correctly performed trials was used for analyses. Psychomotor speed and attention was assessed by the trails A task which requires connecting disarrayed digits (1 to 25) in sequence after familiarization with the task using an 8 digit example. Switching of attention was assessed by the trails B task which requires connecting disarrayed digits (1 to 13) and letters (A to L) alternatively in sequence and familiarization with the task using a 4 digit, 4 letter example. The difference in completion time between the trails B and A tasks assesses shifting of attention and was used for analyses.

EEG preprocessing and source localization

Offline preprocessing of recordings was conducted using a custom MATLAB pipeline calling selected functions from the EEGLAB toolbox.(3) In general terms, preprocessing proceeded as follows: EEG data were downsampled to 250 Hz, notch filtered to remove 60 Hz line noise and its harmonic, and bandpass filtered between 1 Hz and 50 Hz using a zero-phase finite impulse response filter. Bad channel (mean 0.9, SD 2.3 rejected channels) and paroxysmal segment (mean 96.5, SD 6.8, percent time points retained) rejections were performed in a semi-automatic manner, assessing extreme or flatline amplitudes, channel correlations,(4) and robust paroxysmal spike measures with custom pipelines and EEG expert validation. Rejected channels were spherically interpolated and paroxysmal segments excised. To remove remaining artifacts including ocular, heartbeat, and high-frequency persistent muscle artifact, the extended information maximization (Infomax) algorithm,(5) widely used for independent components analysis (ICA), was then performed on the data reduced in dimensionality by principal components analysis (PCA). The number of the dimensions was determined to be the least

number of principal components that account for more than 99.9% of the total variance. Artefactual independent components were likewise identified by combination of custom pipelines identifying extreme skew in component topographical weights, stereotypical power spectral density profiles, deviant robust statistics, etc., confirmed by EEG expert, and then rejected.(6–8)

Source localization to the cortical surface was performed using the Brainstorm toolbox.(9) A three-layer symmetric boundary element model (BEM) of the head was computed with the OpenMEEG(10, 11) plugin based on a Montreal Neurological Institute (MNI) brain template. Rotating dipoles at 5003 vertices were generated on the cortical surface. The lead-field matrix was obtained by projecting the standard electrode positions onto the scalp. For each subject, an imaging kernel that maps from the channel space EEG to the source-space current density was then estimated by the minimum norm estimation (MNE) approach with depth weighting and regularization. For the noise covariance estimation, we assumed the noise in different channels were uncorrelated with equal variance. We selected the MNE approach over beamforming techniques as dynamical imaging of coherent sources(12) or linearly constrained minimum variance beamforming techniques (as used by Hipp, et. al.) are sensitive to inaccuracy in forward modeling, which is more of an issue for EEG than for MEG due to the volume conduction.(13)

For each vertex, the current density time series were reduced from their 3 orthogonal axes to a single principal direction by PCA, then bandpass filtered into canonical frequency bands associated with different neurophysiological processes: theta (4-7 Hz), alpha (8-12 Hz), beta (13-30 Hz), and gamma (31-50 Hz). The current density time series at each canonical frequency band were Hilbert transformed to yield source-space analytical time series. Welch's periodogram was calculated in source-space to generate the power spectral density for comparison with the orthogonalization method.

Summary of orthogonalization workflow

The EEG signal is acquired with 64 channels over 3 minutes (Figure S1a). Using a BEM and MNE (Figure S1b), source localization is performed using the MNI template brain (Figure S1c). An unconstrained spatial imaging kernel (W) is obtained (Figure S1d) and is reduced by PCA to a single principal direction (K), one value per vertex (Figure S1e). This spatial imaging kernel is multiplied by the analytic signal, obtained from band-passed and Hilbert transformed EEG data, to yield the source-space data (Figure S1f).

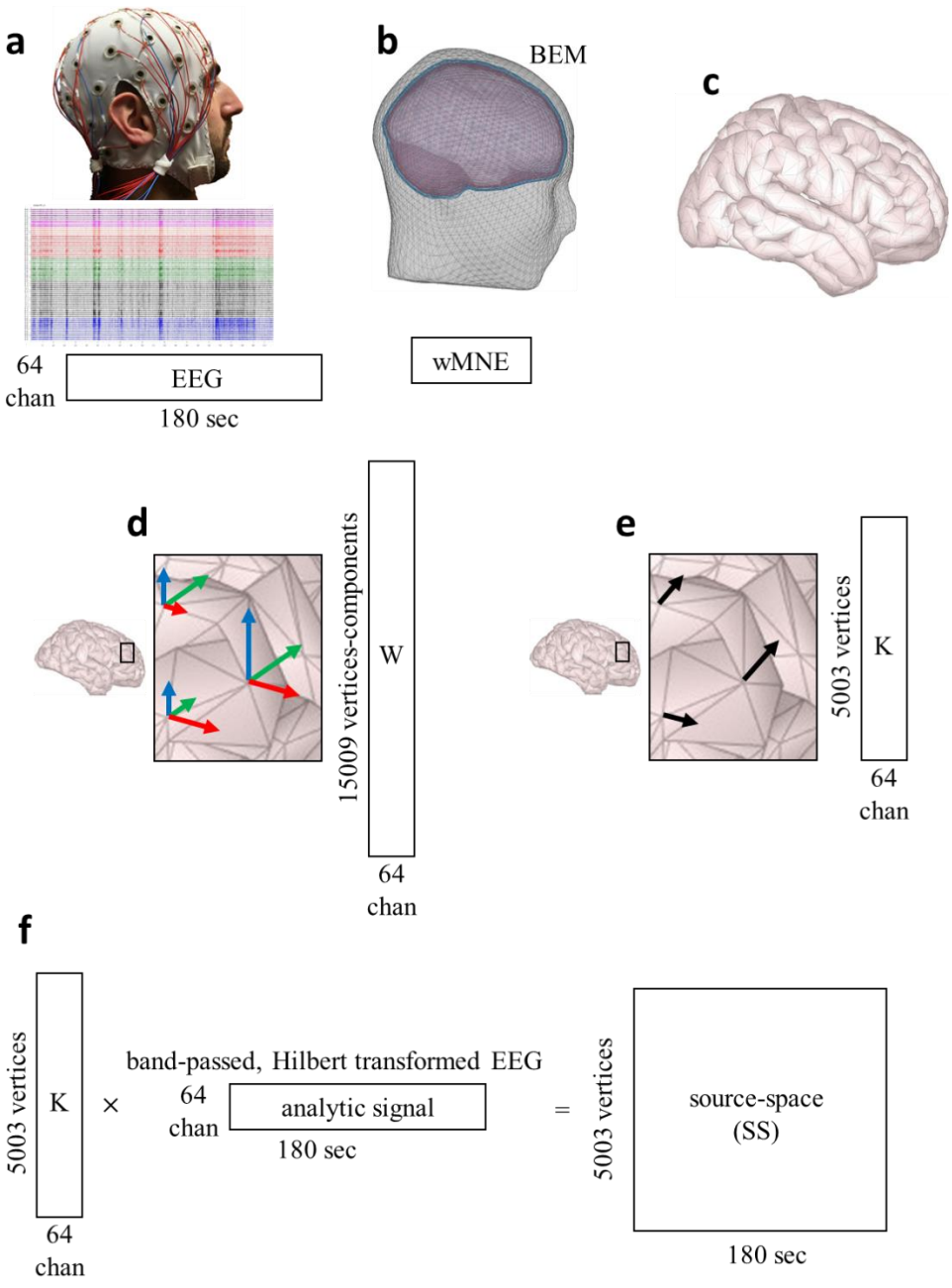

FIGURE S1. Orthogonalization Workflow: EEG to Source-Space.

(a) 3 minutes of 64 channel EEG data is acquired and preprocessed to remove artifacts. (b) This EEG data is combined with a boundary element model forward solution to enable use of weighted minimum norm estimation applied to 5003 vertices (c) of the Montreal Neurological Institute template brain. (d) 3 orthogonal dipoles (x,y,z axis) are estimated at each vertex of source-space to produce a spatial imaging kernel (W) of 15,009 dipole components across the 64 channels. (e) These dipole components are reduced by principal components analysis to yield a spatial imaging kernel (K) of one dipole per vertex (constrained solution). (f) This new kernel (K) is then multiplied by the band-limited, analytic EEG signal to produce the source-space used in analysis.

Representative vertices, red and blue, from this source-space (Figure S2a) illustrate the orthogonalization procedure. At each time point, the signals may be represented in the complex plane (Figure S2b). Here, the perpendicular (orthogonal) component seen as the magenta signal, results from the blue signal being orthogonalized with respect to the red signal. The shared, parallel component (brown) represents the trivial covariability shared as a result of volume conduction. The resulting power envelopes of these signals is seen in Figure S2c. The natural logarithms of these signals are then correlated to produce a measure of connectivity between the 2 vertices (Figure S2d).

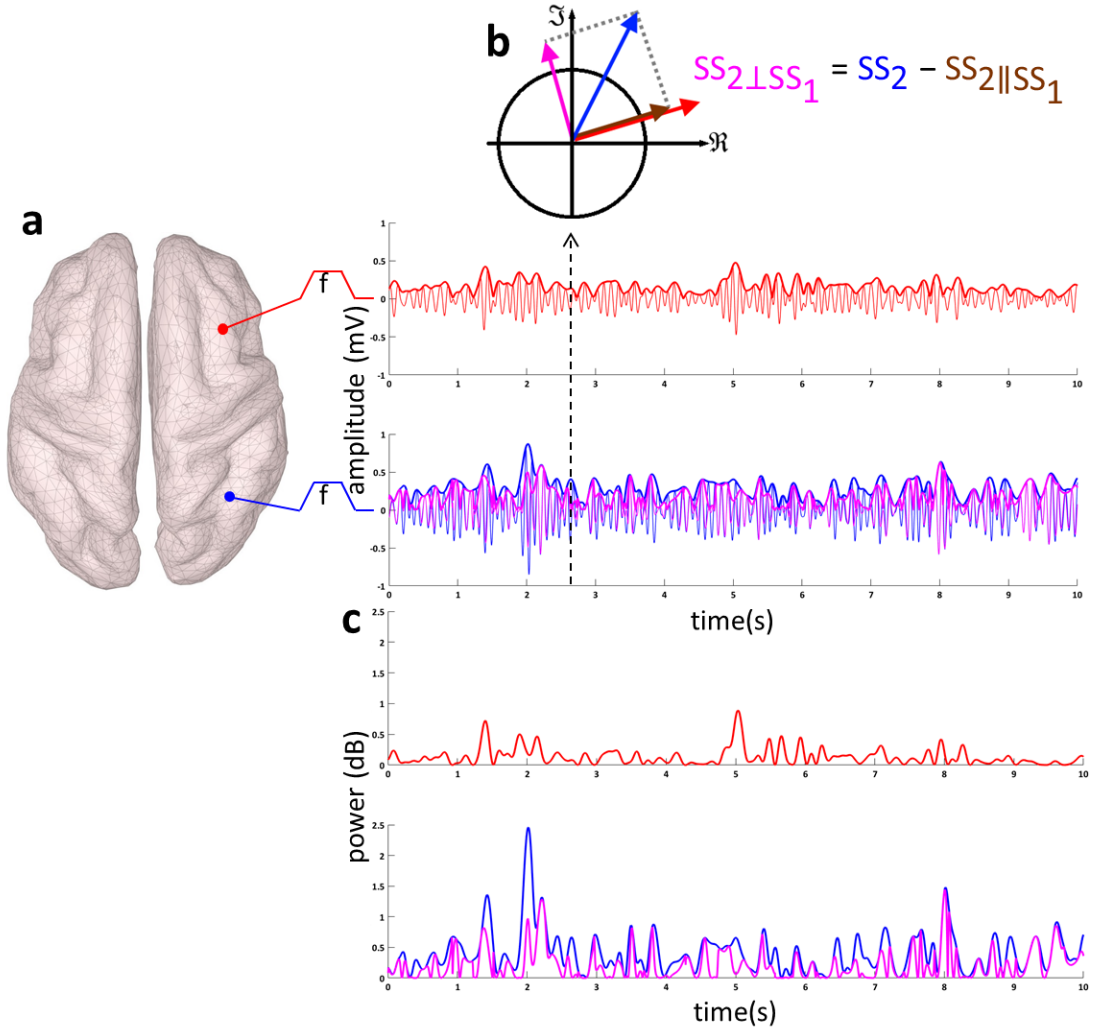

d $corr(log(PE_1), log(PE_2)) = .17$

$corr(log(PE_1), log(PE_{2\perp PE1})) = .08$

FIGURE S2. Orthogonalization Workflow: Example Using 2 Vertices.
(Continued)

(a) To demonstrate the orthogonalization method's application, the time series of 2 vertices of source-space, signal 1 in red and signal 2 in blue, are illustrated. (b) As these signals are analytic (i.e., complex-valued), at each time point they may be represented as vectors in the complex plane. Signal 2 orthogonalized with respect to signal 1 produces the magenta, perpendicular (hence orthogonal) vector. The brown, parallel component represents volume conduction, which this method effectively removes. (c) The power envelopes of these resulting signals demonstrate that the magenta, orthogonalized signal is now smaller in amplitude than the original, blue signal 2 as volume conduction's contribution has been subtracted. (d) The stronger correlation between the original signals is attributable to volume conduction and the smaller correlation value of now .08 represents the true physiological covariation between the brain sources.

At scale, this procedure is implemented iteratively and is ideally parallelized for computation on a graphics processing unit. Plain power envelopes are obtained from source-space (Figure S3a-b). Then all of source-space is orthogonalized with respect to 1 vertex (Figure S3c) and orthogonalized power envelopes are obtained (Figure S3d). The natural logarithm of these 2 sets of power envelopes are then correlated (Figure S3e) to obtain 1 column of the connectivity matrix (Figure S3f). This procedure is iterated, orthogonalizing with respect to successive vertices (Figure S3g-i) until the entire connectivity matrix is obtained (Figure S3j).

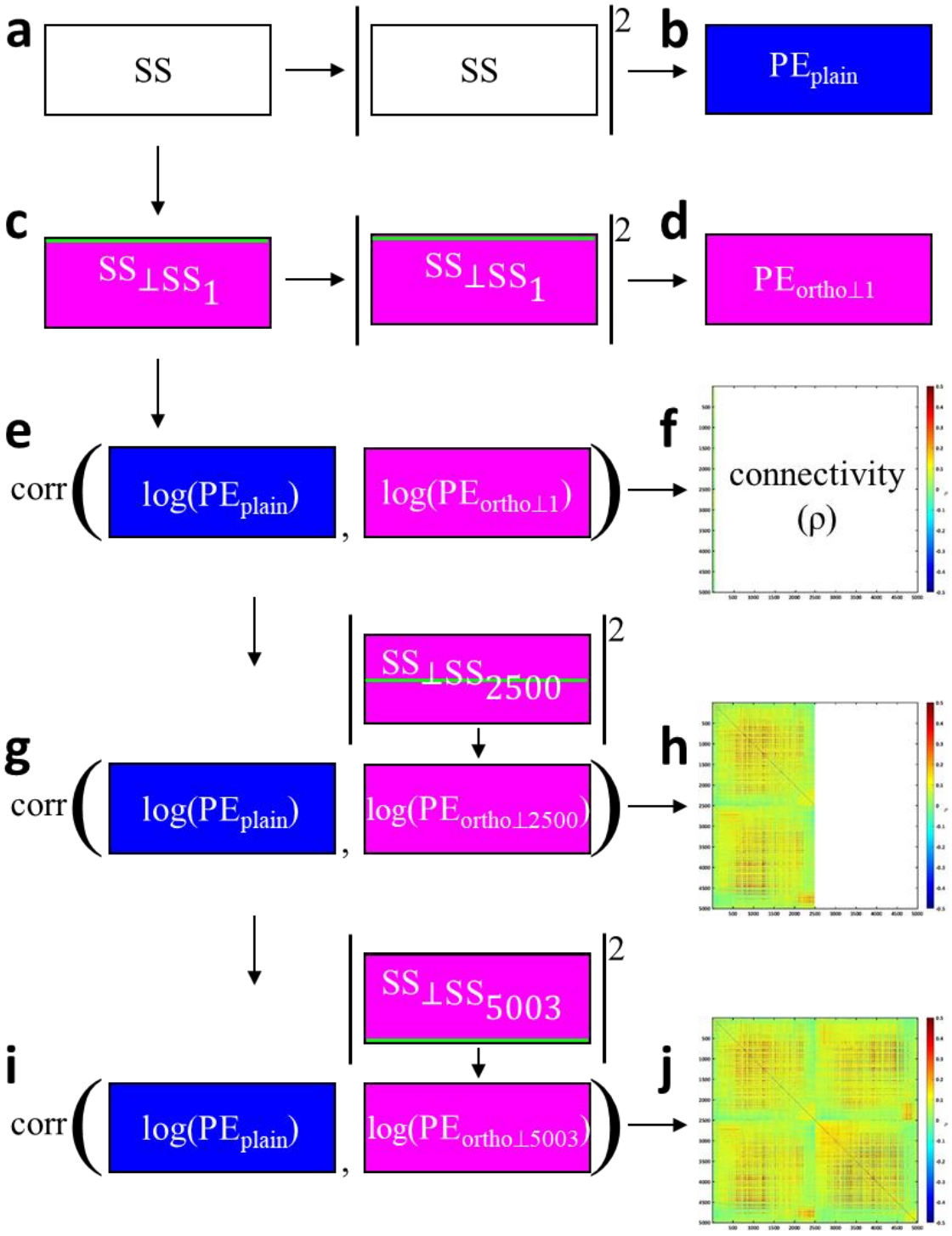

FIGURE S3. Orthogonalization Workflow: Iterating the Procedure to Produce a Connectivity Matrix. (a) Source-space (SS) is used to calculate plain power envelopes (b) PEplain. (c) All of SS is then orthogonalized with respect to vertex 1 and this orthogonalized SS is used to calculate (d) orthogonalized power envelopes (PEortho). (e) The correlation coefficients of these power envelopes,

log-transformed to render them more normal, produce 1 column of the (f) connectivity matrix, representing the correlation of vertex 1 with every vertex of the brain. (g-h) This process is then iterated, illustrated at the procedure's midpoint, orthogonalizing with respect to vertex 2500 and is completed (i-j) in orthogonalizing with respect to the last vertex, 5003. As each iteration is not dependent on any other, this process is ideally parallelized and well-suited for graphical processing unit-based computation.

Machine Learning

In order to assess the detection power of the orthogonalized power envelope connectivity as a biomarker, we used the connectivity values as features to train a machine learning classifier to distinguish PTSD patients from trauma-exposed controls. Specifically, we implemented classification with cross-validation to validate the efficacy of our exploratory biomarker on predicting independent PTSD samples. A linear kernel-based relevance vector machine was applied to train the classifier for identification of PTSD participants from health controls (14) Classification performance was evaluated first using a leave-one-out cross-validation procedure. To further confirm the generalization capability of the biomarker, we also implemented a 10x10-fold cross-validation for classification and ROC analysis in the current revision. Specifically, we randomly divided all participants into 10 folds in 10 different orders. In each order, one fold was left out as test set while the remaining nine folds were used for classifier training. This was repeated 10 times so that each fold was left out only once for testing. The classification performance was evaluated by comparing the predicted labels and the true ones, and then averaged over all the 10 orders.

The MATLAB function we employed in this analysis is provided below.

Implementing the orthogonalization procedure in MATLAB

```
function [Rplain,Rortho] = orthogonalize(K,BPCD)
% This function calculates the orthogonalized connectivity matrix (Rortho)
% as well as the plain (non-orthogonalized) connectivity matrix (Rplain)
% given a spatial imaging kernel (K) and band-passed complex EEG data (BPCD)
%
% K is a matrix obtained from an inverse solution method such as minimum norm
% estimation using the Brainstorm toolbox. It has dimensionality v vertices x n
% channels.
%
% BPCD is a complex matrix of EEG data that has been band-passed at a certain
% center frequency and bandwidth. For example, EEG data band-passed with center
% frequency 10 Hz and bandwidth 4 Hz to contain the alpha frequency band. This
% data is then made into an analytic signal via the Hilbert transform or using
% Morlet wavelets, etc. It has dimensionality n channels x t time points.

% 1. Input validation.

% 1.1. K and BPCD are required inputs
narginchk(2,2)
```

```
% 1.2. K and BPCD must be matrices.
assert(ismatrix(K),'K must be a matrix (vertices x channels).')
assert(ismatrix(BPCD),'BPCD must be a matrix (channels x time points).')

% 1.3. BPCD must be complex-valued.
assert(~isreal(BPCD),'BPCD must be a complex-valued matrix.')

% 1.4. K and BPCD must not have any non-finite values (NaNs).
assert(all(isfinite(K(:))),'Non-finite values detected in K.')
assert(all(isfinite(real(BPCD(:)))),'Non-finite values detected in BPCD.')
assert(all(isfinite(imag(BPCD(:)))),'Non-finite values detected in BPCD.')

% 1.5. Issue a warning if the imaginary component of BPCD is all zero or near
% zero values.
if nansum(nansum(round(imag(BPCD),3))) == 0
   warning('The imaginary component of BPCD appears to contain all zero values,
check that your band-passed complex EEG data is correct.')
end

% 2. Calculate source space (SS). Dimensionality is v vertices x t time points.
% Values are computed using single precision as the memory and computation time
% requirements increase substantially when using double precision with
% negligible gain in accuracy.
SS = single(K * BPCD);

% 3. Initialize the directional connectivity matrix (RorthoAB). Dimensionality
% is a square matrix of v vertices x v vertices.
RorthoAB = single(NaN(size(K,1),size(K,1)));

% 4. Determine if a capable GPU is present to perform the orthogonalization.
toolboxInfo = ver;
useGPU = false;
% The Parallel Computing Toolbox is required to use GPU functions.
if any(strcmp({toolboxInfo.Name},'Parallel Computing Toolbox'))
   if gpuDeviceCount > 0
      gpu = gpuDevice(1);
      SSinfo = whos('SS');
      RorthoABinfo = whos('RorthoAB');
      % Check to make sure the detected GPU has enough available memory.
      if gpu.AvailableMemory >= 2 * SSinfo.bytes + RorthoABinfo.bytes
         useGPU = true;
      else
         warning('A GPU was detected, but it does not have sufficient memory. Using
the CPU to perform the orthogonalization. This will take substantially longer
computation time (possibly an hour or more).')
      end
   else
      warning('No GPU was detected, using the CPU to perform the orthogonalization.
This will take substantially longer computation time (possibly an hour or more).')
   end
else
   warning('No Parallel Computing Toolbox was detected (required to use GPUs).
Using the CPU to perform the orthogonalization. This will take substantially longer
computation time (possibly an hour or more).')
end
```

```
% 5. Calculate the plain power envelopes (PEplain) by multiplying SS with its
% conjugate. Dimensionality is v vertices x t time points.
PEplain = SS .* conj(SS);

% 6. Calculate the plain connectivity matrix (Rplain) by computing the
% vertex-wise correlations of the natural logarithm of the plain power
% envelopes (PEplain). A small value (tol) is added to the power envelopes to
% prevent the natural logarithm resulting in a non-finite value (i.e., to prevent
% log(0) = -Inf). Dimensionality is a square matrix of v vertices x v vertices.
tol = single(1e-9);
Rplain = corr(log(PEplain' + tol),log(PEplain' + tol));

% 7. Calculate the directional orthogonalized connectivity matrix (RorthoAB).
% Here, AB refers to the fact that orthogonalization is a directional operation.
% That is, vertex A orthogonalized with respect to vertex B is not the same as
% vertex B orthogonalized with respect to vertex A. This is accomplished by
% orthogonalizing SS with respect to one vertex per iteration, calculating
% the resulting orthogonalized power envelopes (PEortho) and the power envelope
% of the seed vertex (PEseed), and then computing the correlation of the natural
% logarithms of these power envelopes to obtain a measure of connectivity. As
% with the correlation of the natural logarithm of the plain power envelopes, a
% small value (tol) is added to prevent non-finite values.
if useGPU
   SS = gpuArray(SS);
   RorthoAB = gpuArray(RorthoAB);
   tol = gpuArray(tol);
end
% Display a waitbar to indicate progress.
waitbarHandle = waitbar(0,'Initializing','Name','Orthogonalized connectivity');
for iVertex=1:size(SS,1)
   % Seed is the vertex that SS is being orthogonalized with respect to.
   % Dimensionality is 1 x t time points.
   seed = SS(iVertex,:);

   % Calculate PEseed by multiplication with its conjugate.
   % Dimensionality is 1 x t time points.
   PEseed = seed .* conj(seed);

   % Calculate PEortho by applying Hipp's equation.
   % Dimensionality is v vertices x t time points.
   PEortho = imag(SS .* ( conj(seed) ./ abs(seed) )).^2;

   % Calculate the correlation between the natural logarithm of PEseed
   % and the natural logarithm of PEortho. This produces a column vector
   % of v correlation coefficients per iteration.
   RorthoAB(:,iVertex) = corr(log(PEseed' + tol),log(PEortho' + tol));

   % Update status bar.
   if mod(iVertex,10) == 0
      waitbar(iVertex/size(SS,1),waitbarHandle,sprintf('Calculating orthogonalized
connectivity.\nVertex %u of %u complete.',iVertex,size(SS,1)));
   end
end
delete(waitbarHandle);
```

```
if useGPU
   RorthoAB = gather(RorthoAB);
   tol = gather(tol);
   reset(gpu);
end

% 8. Calculate the symmetric, corrected orthogonalized connectivity matrix
% (Rortho). For region of interest intersection connectivity analyses, a
% symmetric connectivity matrix is required. Therefore, RorthoAB is averaged
% with its transpose. Due to underestimation of correlation inherent to
% orthogonalization, a correction factor of 0.578499 is applied. See Hipp,
% J.F. et al., 2012. Large-scale cortical correlation structure of spontaneous
% oscillatory activity. Nature Neuroscience, 15(6), pp.884-890. for the basis of
% this.
Rortho = ((RorthoAB + RorthoAB') ./ 2) ./ 0.578499;

% 9. Limit the correlation values of Rplain and Rortho to |1 - tol|. This is
% done to prevent non-finite values in the Fisher R to Z transform of the
% correlation coefficients (i.e., fisherz(1) = Inf).
Rplain(Rplain >= 1) = 1 - tol;
Rplain(Rplain <= -1) = -1 + tol;
Rortho(Rortho >= 1) = 1 - tol;
Rortho(Rortho <= -1) = -1 + tol;
end
```

All other scripts and procedures (such as construction of the linear mixed effects models, etc.) will be shared upon request by contacting the corresponding author.

Region of interest parcellation

Significant clusters of activation are identified by ICA in fMRI resting-state scans (Figure S4a-c). These clusters are projected onto the MNI template along with anatomically defined somatosensory and visual regions of interest to produce the atlas used for these analyses (Figure S4d). Thus, the initial fMRI clusters (Figure S4e) are thresholded (Figure S4f) and their corresponding vertices in the connectivity matrix is used to determine the mean region of interest (ROI) pair correlation as their measure of connectivity (Figure S4g).

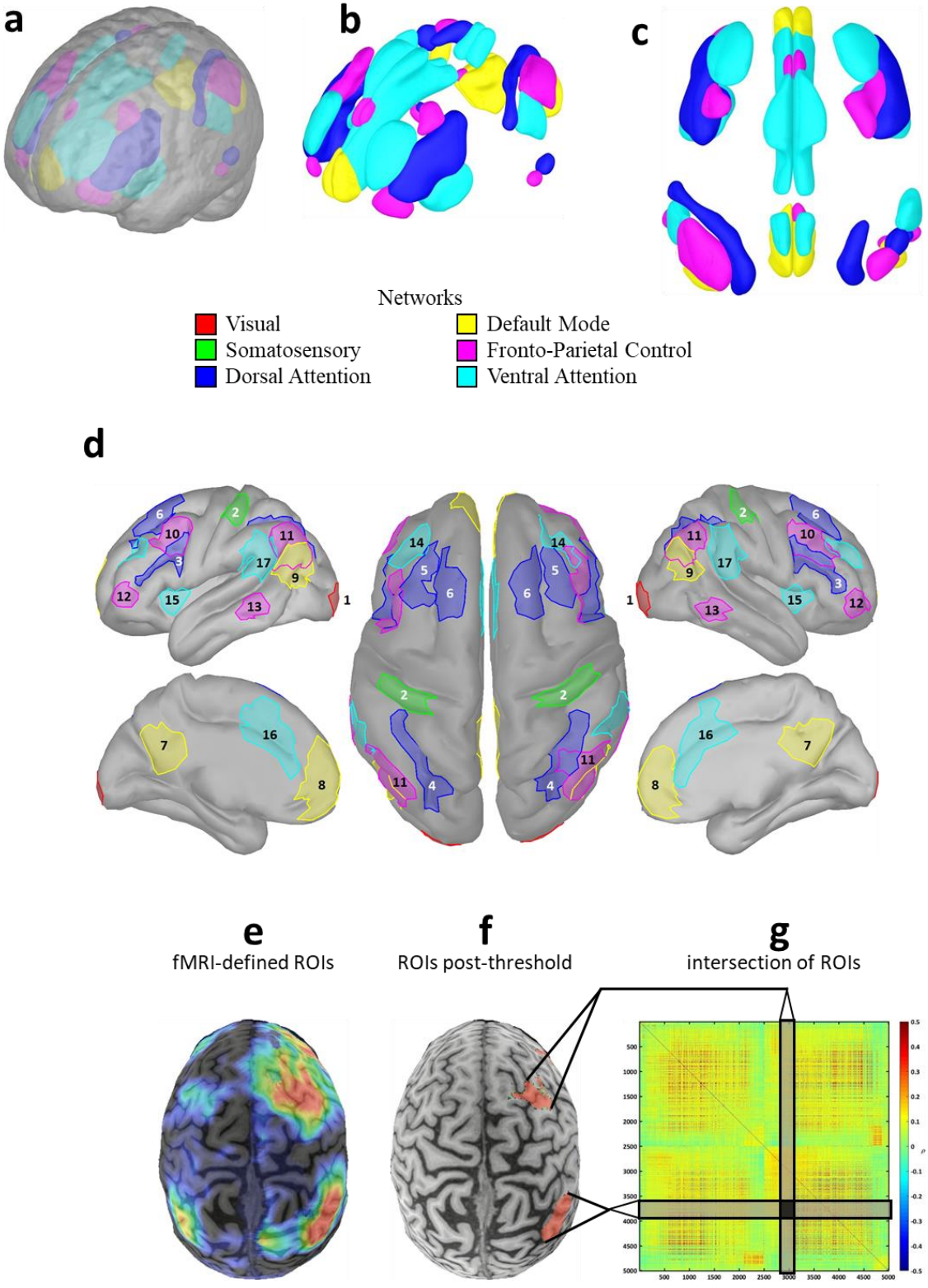

FIGURE S4. Region of Interest Parcellation.
(Continued)

(a) 31 regions of interest (ROIs) in 6 cortical networks were defined in Montreal Neurological Institute (MNI) space, derived from independent components analysis parcellation of resting-state functional MRI connectivity from 38 subjects in a separate study. This was done to ground our EEG ROIs in a commonly-used, fMRI-derived definition of the major cortical connectivity networks. (b-c) Oblique and dorsal views of the initial fMRI clusters. (d) These clusters were projected to the cortical source-space representation of the MNI brain. Numbering and abbreviations: Visual Network: 1. Visual Area 1 (V1); Somatosensory Network: 2. Somatosensory Cortex (SMC); Dorsal Attention Network: 3. Inferior Frontal Junction (IFJ), 4. Intraparietal Sulcus (IPS), 5. Frontal Eye Fields (FEF), 6. Supplemental Eye Fields (SEF); Default Mode Network: 7. Posterior Cingulate Cortex (PCC), 8. Medial Prefrontal Cortex (MPFC), 9. Angular Gyrus (ANG); Frontoparietal Control Network: 10. Posterior Middle Frontal Gyrus (PMFG), 11. Inferior Parietal Lobule (IPL), 12. Orbital Gyrus (ORB), 13. Middle Temporal Gyrus (MTG); Ventral Attention Network: 14. Anterior Middle Frontal Gyrus (AMFG), 15. Insula (INS), 16. Dorsal Anterior Cingulate Cortex (DACC), 17. Supramarginal Gyrus (SUP). To summarize the process from fMRI map to connectivity matrix, a fMRI map (e) of the frontoparietal control network is used to identify the PMFG and IPL (f). The intersection of the constituent vertices of these ROIs (g) is used to obtain the values from which mean correlation (connectivity) is defined.

RESULTS

Healthy control methods validation study, no mean subtraction

Subtraction of mean connectivity, as performed by Hipp, et. al., is useful in distinguishing a particular seed or ROI's connectivity topography distinct from the brain-wide average connectivity. However, this method is typically dominated by stronger bilateral medial topographies and can suppress more distributed topographies. Figure S5 describes the same processes of analyzing the functional network connectivity patterns in our validation set of 36 healthy civilian controls as described in Figure 2, with the exception that here we calculate the T statistic from mean ROI connectivity > 0 rather than mean ROI connectivity > brain-wide average connectivity and calculate the one-tailed P value as done by Hipp, et. al.

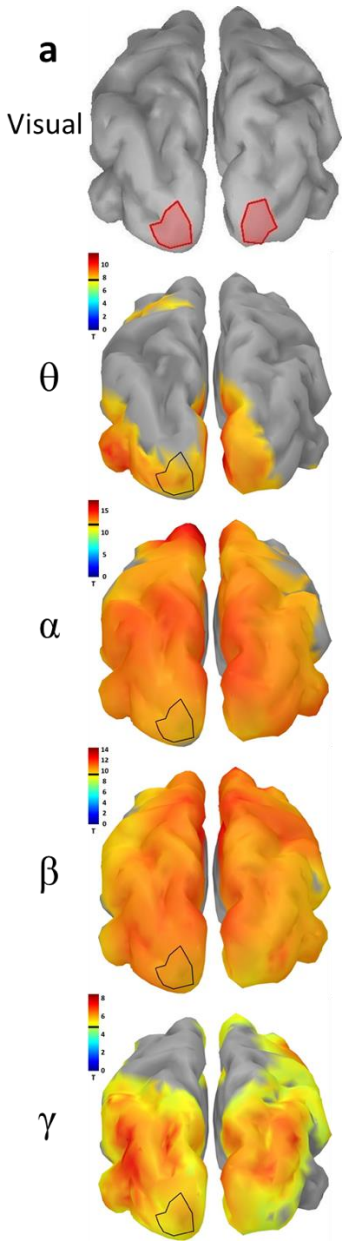

FIGURE S5. Functional Connectivity Patterns Revealed Using Orthogonalized Resting EEG Power Envelopes, No Mean Subtraction.

In our validation sample of 36 healthy civilians, the T test for correlation > 0 ($pFDR_{3000\ vertices} < .05$, right-tailed) illustrates connectivity for each of the 3000 vertices calculated from the region of interest (ROI) seeds outlined in black. In contrast to Figure 2, this method illustrates the broader topographies of the functional networks. The constituent regions of each network are represented above the network topographies obtained in the theta, alpha, beta, and gamma frequency bands. These connectivity maps were likewise generated in the eyes open condition. The black bar on each colorbar depicts the arbitrary threshold set for optimal visualization of the network's topography.

(a) Seeding the left visual cortex (V1) reveals the visual network with more focal topographies in the theta and gamma frequency bands.

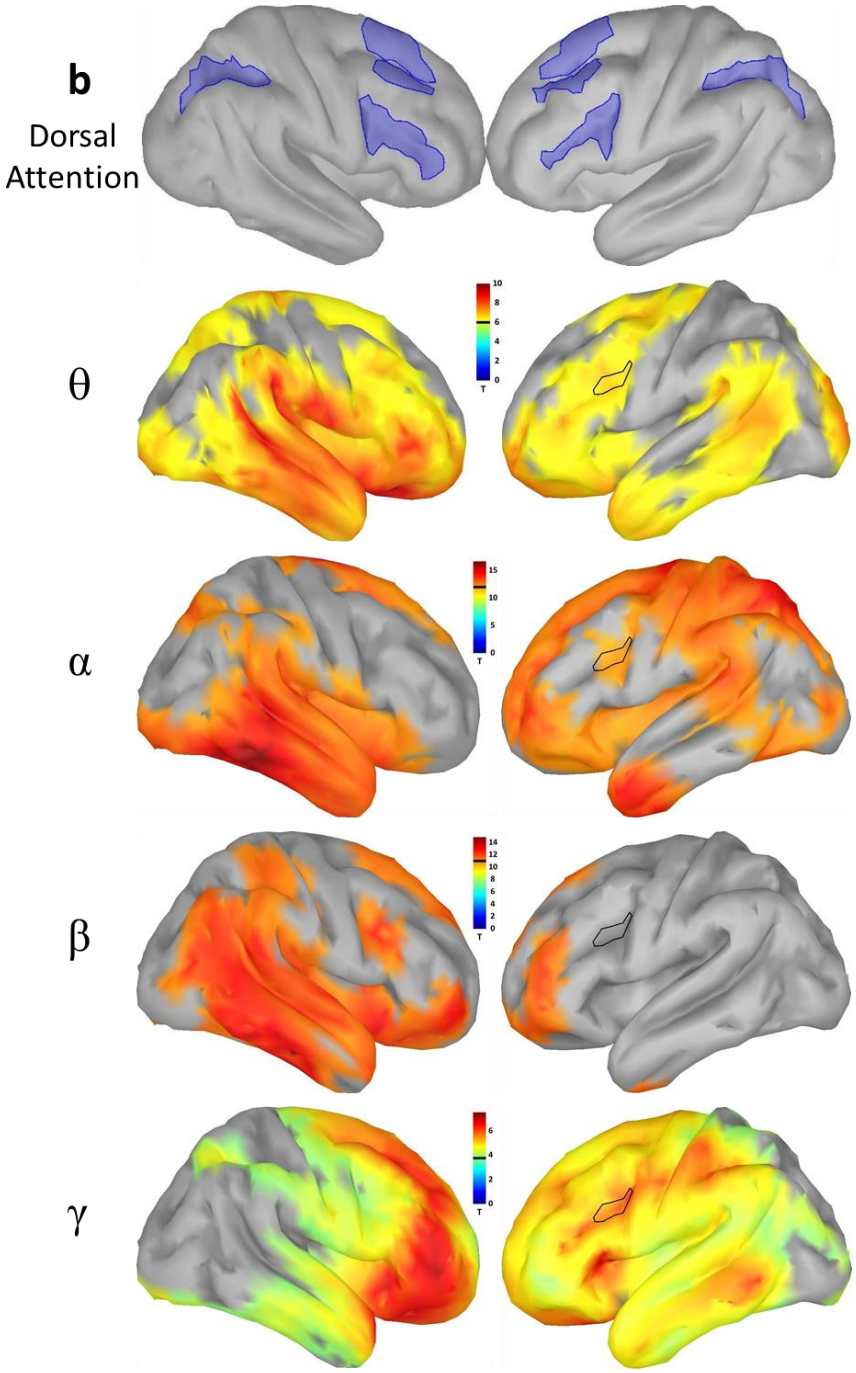

(b) Seeding the left inferior frontal junction produces bilateral inferior frontal junction and frontal eye field connectivity in the theta frequency band and bilateral supplemental eye field connectivity in the alpha frequency band. In the beta frequency band, contralateral inferior frontal junction connectivity is observed as is bilateral connectivity between the inferior frontal junctions, frontal and supplemental eye fields, and intraparietal sulcus in the gamma frequency band.

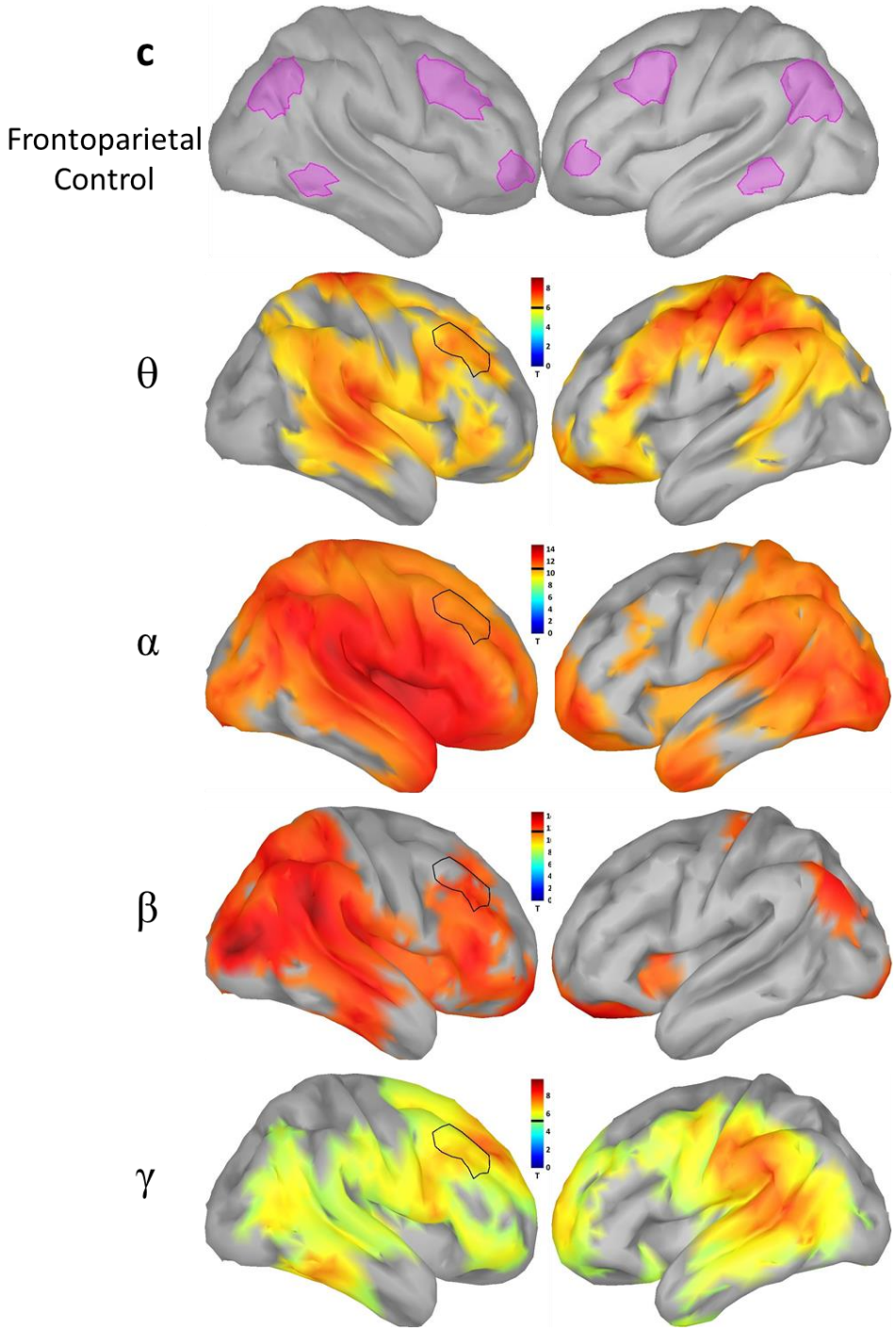

(c) Seeding the right posterior middle frontal gyrus reveals connectivity across all frequency bands with contralateral homologue (excepting beta frequency band) and regions near the orbital gyri and bilateral inferior parietal lobules.

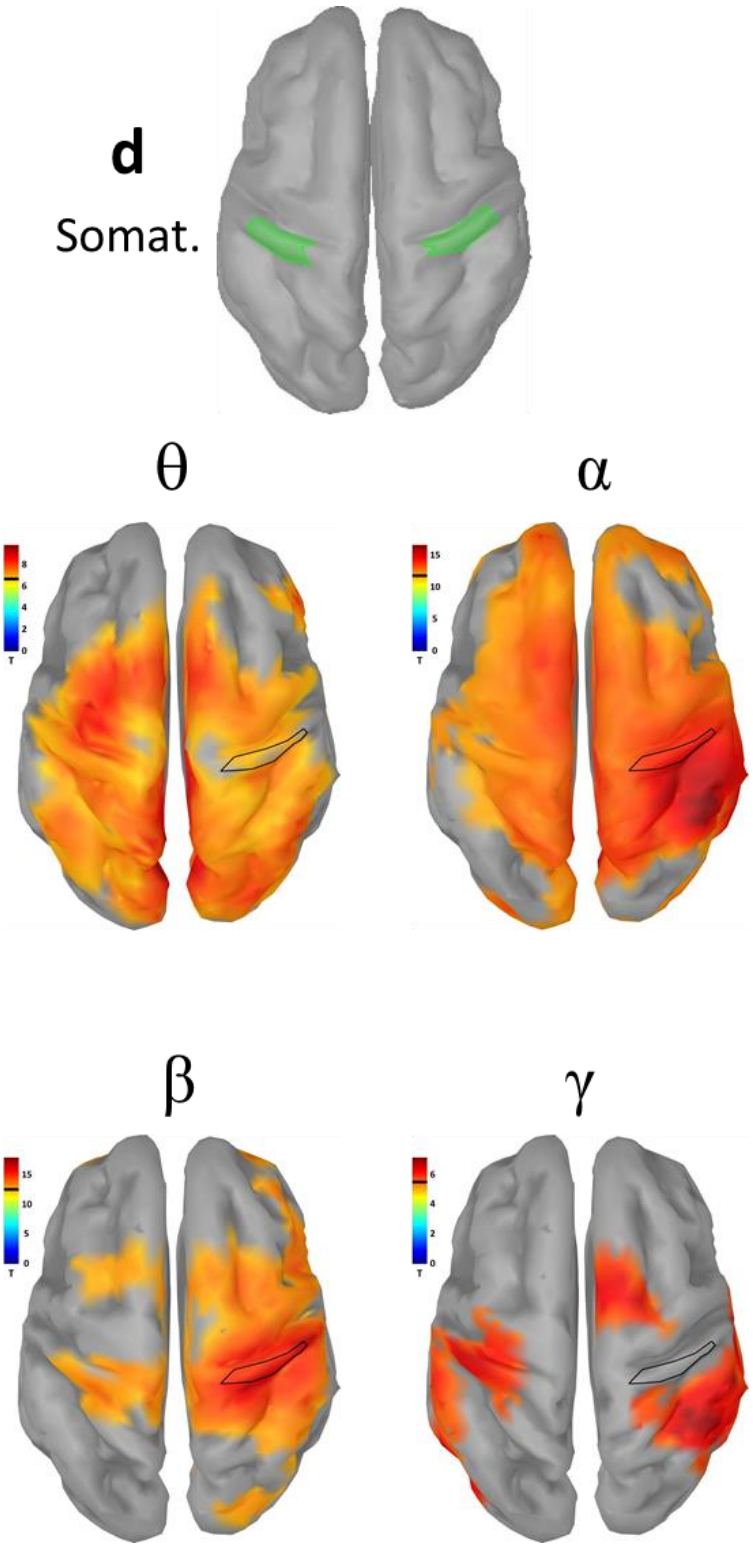

(d) Seeding the right somatosensory cortex shows the symmetric topography of the somatosensory network, with more focal topographies observed in the beta and gamma frequency bands.

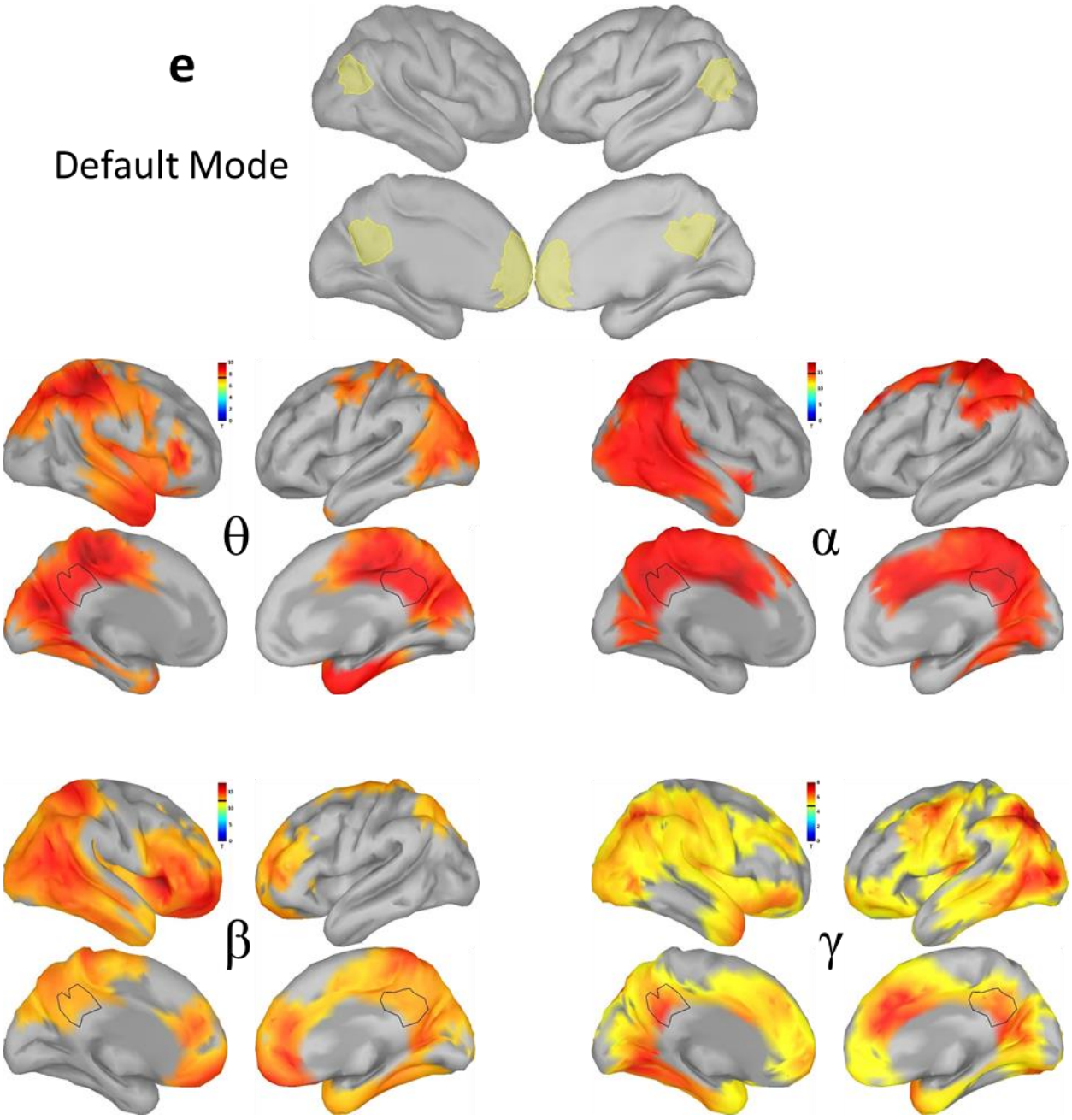

(e) Seeding the posterior cingulate demonstrates connectivity with the angular gyri but not with the medial prefrontal cortex in the theta and frequency bands. However, connectivity to the medial prefrontal cortex is pronounced in the beta frequency band and emerges to a lesser degree in the gamma frequency band.

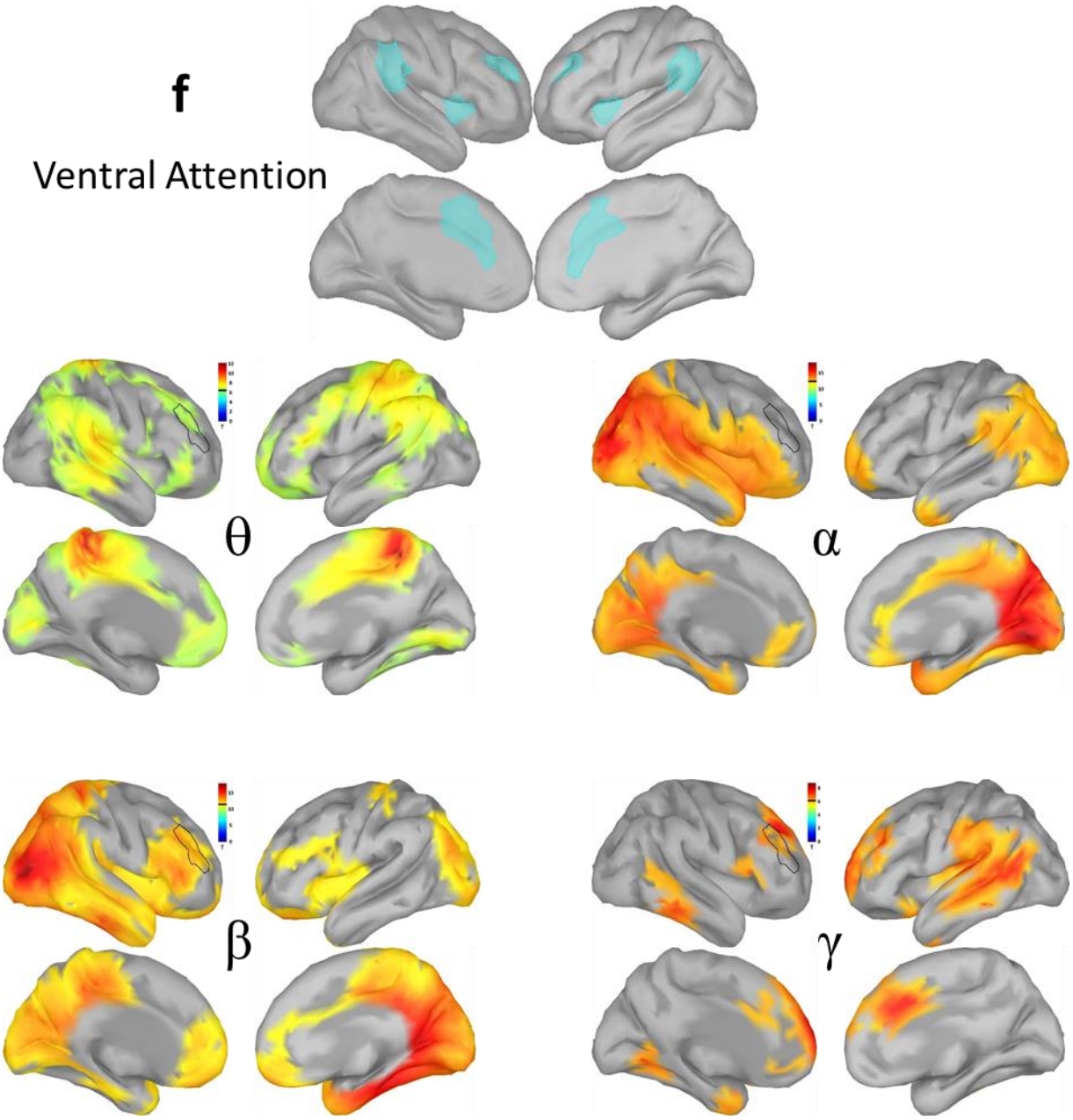

(f) Seeding the right anterior middle frontal gyrus shows bilateral connectivity with the contralateral homologue and bilateral supramarginal gyri as well as connectivity with the dorsal anterior cingulate cortex in the theta and alpha frequency bands. Bilateral anterior middle frontal gyri and insula connectivity is observed in the beta frequency band, with some ipsilateral connectivity to supramarginal gyrus and dorsal anterior cingulate gyrus. The gamma frequency band demonstrates a more focal connectivity topography between anterior middle frontal gyri, ipsilateral insula and dorsal anterior cingulate gyrus, and contralateral supramarginal gyrus.

TABLE S1. Intranetwork - Extranetwork Connectivity, No Mean Subtraction								
	Frequency Bands, T Statistic (P Value)							
Functional Networks	Theta		Alpha		Beta		Gamma	
Visual	**4.18**	**(< .001)**	**5.22**	**(< .001)**	**5.59**	**(< .001)**	1.78	(0.13)
Somatosensory	**2.88**	**(0.02)**	**4.81**	**(< .001)**	**6.82**	**(< .001)**	0.82	(0.46)
Dorsal Attention	-1.85	(0.12)	0.08	(0.94)	2.28	(0.06)	-0.93	(0.43)
Default Mode	1.31	(0.26)	**5.40**	**(< .001)**	**6.77**	**(< .001)**	0.85	(0.46)
Frontoparietal Control	-1.27	(0.27)	**-3.81**	**(0.00)**	-1.94	(0.10)	1.97	(0.10)
Ventral Attention	-0.39	(0.73)	-1.37	(0.25)	-2.2	(0.07)	**3.55**	**(0.00)**

Table S1 reproduces the same analyses as Table 2, but again, compares mean ROI connectivity to 0 rather than the brain-wide mean. Significant intranetwork minus extranetwork differences are observed in the same frequency band-network pairs as in Table 2.

Connectivity differences in PTSD

Selected ROI pairs within the theta frequency band demonstrate consistent hypoconnectivity in the PTSD group compared to controls.

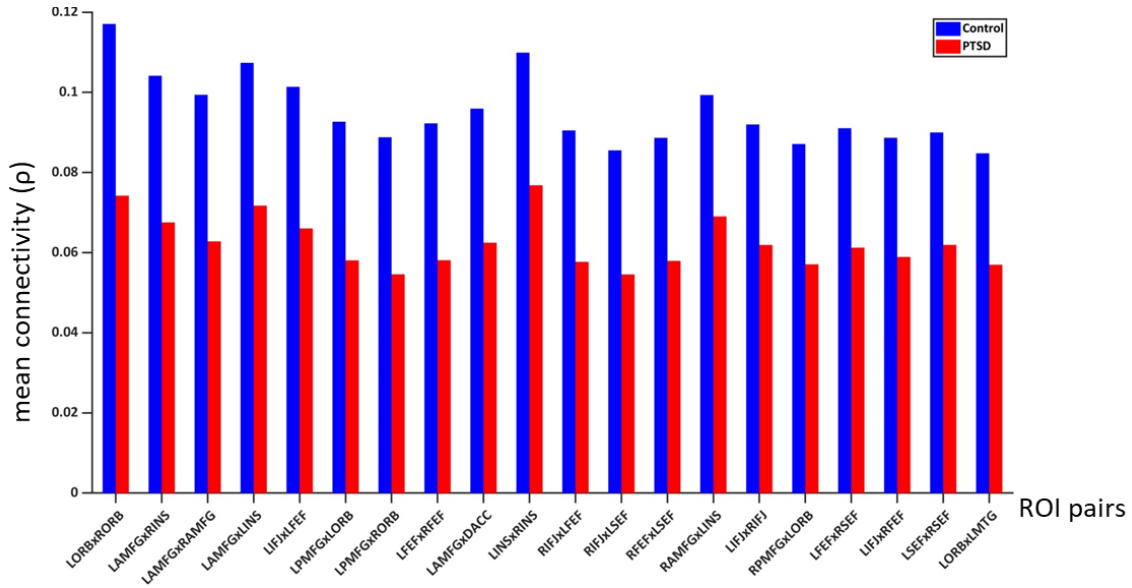

FIGURE S6. Contrast of mean connectivity values between control (blue) and PTSD (red) from selected ROIs in the theta frequency band.

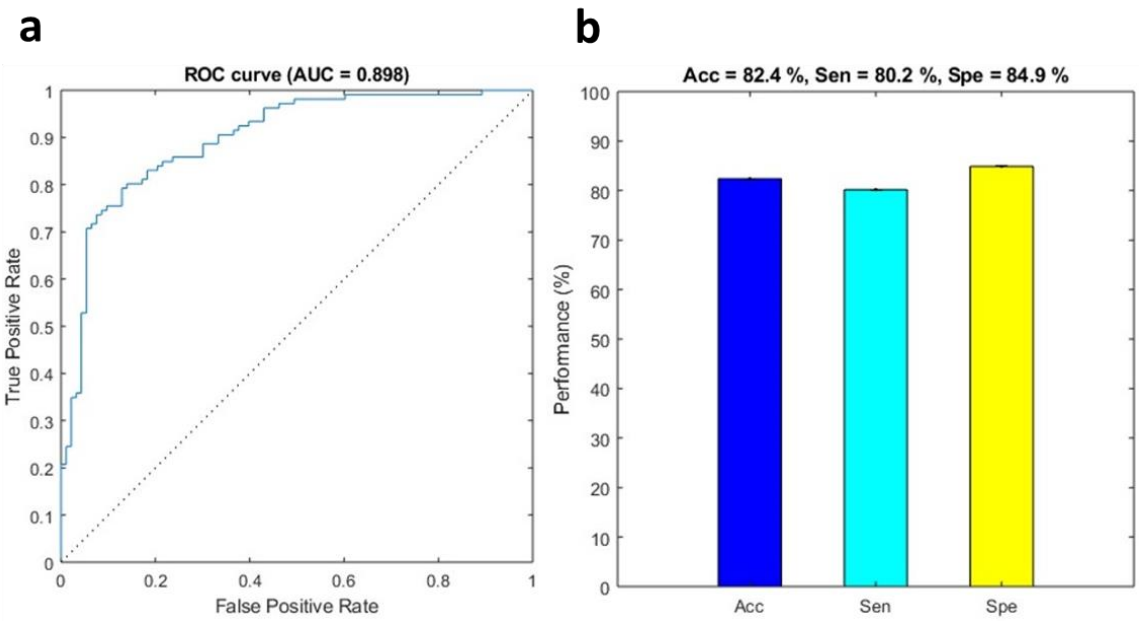

FIGURE S7. Orthogonalized Connectivity Values as Features for Training a Machine Learning Algorithm using leave-one-out cross-validation.

Comparison of directionality

The orthogonalization method we applied is a directional operation; that is signal 1 orthogonalized with respect to signal 2 is not the same as signal 2 orthogonalized with respect to signal 1. To compare whether this directionality impacts estimates of connectivity, we contrasted connectivity calculated using each method, but found that differences were exceptionally small and non-significant.

REFERENCES

1. Silverstein SM, Berten S, Olson P, et al.: Development and validation of a World-Wide-Web-based neurocognitive assessment battery: WebNeuro. Behav Res Methods 2007; 39:940–949
2. Paul RH, Lawrence J, Williams LM, et al.: Preliminary validity of "integneuro™": A new computerized battery of neurocognitive tests. Int J Neurosci 2005; 115:1549–1567
3. Delorme A, Makeig S: EEGLAB: An open source toolbox for analysis of single-trial EEG dynamics including independent component analysis. J Neurosci Methods 2004; 134:9–21
4. Bigdely-Shamlo N, Mullen T, Kothe C, et al.: The PREP pipeline: standardized preprocessing for large-scale EEG analysis. Front Neuroinform 2015; 9:1–20
5. Bell AJ, Sejnowski TJ: An Information-Maximization Approach to Blind Separation and Blind Deconvolution. Neural Comput 1995; 7:1129–1159
6. Jung T-P, Makeig S, Humphries C, et al.: Removing electroencephalographic artifacts by blind

source separation. Psychophysiology 2000; 37:163–178

7. Vigário RN: Extraction of ocular artefacts from EEG using independent component analysis. Electroencephalogr Clin Neurophysiol 1997; 103:395–404

8. Ting KH, Fung PCW, Chang CQ, et al.: Automatic correction of artifact from single-trial event-related potentials by blind source separation using second order statistics only. Med Eng Phys 2006; 28:780–794

9. Tadel F, Baillet S, Mosher JC, et al.: Brainstorm: A User-Friendly Application for MEG/EEG Analysis [Internet]. Comput Intell Neurosci 2011; 2011:1–13Available from: http://www.hindawi.com/journals/cin/2011/879716/

10. Gramfort A, Papadopoulo T, Olivi E, et al.: OpenMEEG: opensource software for quasistatic bioelectromagnetics. Biomed Eng Online 2010; 9:45

11. Kybic J, Clerc M, Abboud T, et al.: A common formalism for the Integral formulations of the forward EEG problem. IEEE Trans Med Imaging 2005; 24:12–28

12. Gross J, Kujala J, Hamalainen M, et al.: Dynamic imaging of coherent sources: Studying neural interactions in the human brain [Internet]. Proc Natl Acad Sci 2001; 98:694–699Available from: http://www.pnas.org/cgi/doi/10.1073/pnas.98.2.694

13. Steinsträter O, Sillekens S, Junghoefer M, et al.: Sensitivity of beamformer source analysis to deficiencies in forward modeling. Hum Brain Mapp 2010; 31:1907–1927

14. Tipping ME: Sparse Bayesian Learning and the Relevance Vector Machine. J Mach Learn Res 2001;